THE ASTROPHYSICAL JOURNAL, 367:115–125, 1991 January 20

PHOTOIONIZATION MODELING OF MAGELLANIC CLOUD PLANETARY NEBULAE. I.

M. A. DOPITA[1] AND S. J. MEATHERINGHAM[2]

Received 1990 April 26; accepted 1990 July 10

ABSTRACT

We present the results of self-consistent photoionization modeling of a first sample of 38 Magellanic Cloud planetary nebulae (PN). From these models, we have constructed a Hertzsprung-Russell (H-R) Diagram for the central stars, and we have derived both the chemical abundances and the nebular parameters.

We find that effective temperatures, $T_{\rm eff}$, derived from a nebular excitation analysis, agree well with the temperatures derived by the classical Zanstra method. However, the nebular analysis method allows us to derive the effective temperatures of hot central stars, as well as in the case of the cooler stars to which the Zanstra method is generally restricted. We find a very good linear correlation between log ($T_{\rm eff}$) and the excitation class. From their positions on the H-R diagram, we conclude that the majority of the central stars in this sample have masses between 0.55 and 0.7 $M_\odot$ and are observed during their hydrogen-burning excursion towards high temperatures. Optically thin objects are found scattered throughout the H-R diagram, but tend to have a somewhat smaller mean mass. A few objects are found to have central stars with very high effective temperatures and masses in excess of 0.7 $M_\odot$. These objects tend to be type I PN, with evidence of a third dredge-up episode resulting in correlated He and N abundance enhancements.

The nebular mass of the optically thick objects is closely correlated with the nebular radius, and PN with nebular masses in excess of 1 $M_\odot$ are observed. The velocity of expansion of the nebula is very well-correlated with the position of the central star on the H-R diagram, and is evidence for continual acceleration of the nebular shell during the transition toward high $T_{\rm eff}$.

Excluding the type I PN, the mean abundances derived for the LMC and the SMC agree very well with the mean abundances previously derived from observation of H II regions and evolved radiative supernova remnants.

Subject headings: galaxies: Magellanic Clouds — nebulae: planetary

I. INTRODUCTION

The study of the evolution of planetary nebulae (PN) has been plagued by uncertainties in the distances to these objects. As a consequence, many fundamental parameters remain uncertain. However, these problems can be overcome by the study of the PN in the Large and Small Magellanic Clouds, or by the observation of the objects lying toward the Galactic bulge.

The Magellanic Cloud sample has been the subject of a systematic and detailed study by us and our group in recent years, and data on the diameters, fluxes, expansion velocities, and kinematics have been accumulated (Dopita *et al.* 1985, 1987, 1988; Dopita, Ford, and Webster 1985; Meatheringham *et al.* 1988; Meatheringham, Dopita, and Morgan 1988; Wood, Bessell, and Dopita 1986; Wood *et al.* 1987). This has led to a general understanding of the outlines of the evolutionary sequence (Dopita and Meatheringham 1990).

However, a detailed understanding of the variety of evolutionary behavior, and mass dependence of the preplanetary nebular mass-loss and chemical dredge-up processes can only be obtained from the detailed modeling and spectrophotometric analysis of individual PN. Such models are rare in the literature. The notable optical spectrophotometric studies which have been used to derive chemical abundances are those of Aller *et al.* (1981), Aller (1983), and the major work of Monk, Barlow, and Clegg (1988), who studied 71 objects in all. All of these studies relied upon the empirical ionization correction factor (ICF) method. Aller *et al.* (1987) combined *IUE* spectra with the earlier optical data to demonstrate, with the aid of photoionization models, that carbon shows a very large enhancement in abundance relative to the H II regions in both the LMC and SMC PN, which was interpreted as direct observational evidence for third dredge-up episode in which triple-α products are brought to the surface layers late in the evolution of the asymptotic giant branch (AGB) stars.

In this paper we present the results of a self-consistent photoionization modeling of 38 of the 40 PN for which we have already presented the spectrophotometric results (Meatheringham and Dopita 1991).

II. THE OBSERVATIONAL DATA BASE

We use the spectrophotometric results presented by Meatheringham and Dopita (1991). This data base has the advantage of a good wavelength coverage (~3400–8000 Å), a good sensitivity and dynamic range (>300), and a spectral resolution of ~5 Å, which is more than adequate to resolve important diagnostic lines such as the [S II] 6717, 6731 Å doublet, the [O III] 4363 Å line from Hγ, or the various lines in the range 4686–4740 Å.

The objects observed are almost all drawn from the Sanduleak, MacConnell, and Philip (1978) list, which is a fairly uniform magnitude limited sample. They were chosen to cover the full range of excitation classes and densities exhibited by these brighter Magellanic Cloud PN, and the sample includes some objects with peculiar spectra signatures such as unusually low [O III]/Hβ ratios, or very strong [N II] lines. However, the fainter objects such as the Jacoby PN studied by

[1] Mt. Stromlo and Siding Spring Observatories, Institute of Advanced Studies, The Australian National University.

[2] Laboratory for Astronomy and Solar Physics, NASA Goddard Space Flight Center.

Henry, Leibert, and Boroson (1989), are not well-represented in this sample. We therefore expect that the fainter, more evolved, and optically thin objects will be rare or absent.

III. PHOTOIONIZATION MODELING

a) General Remarks

In order to determine the PN nebular abundances and the position of the central star on the H-R diagram, we require to know only the absolute Hβ flux and the nebular density, and to have accurate spectrophotometry over as wide a wavelength as possible. This is possible because, with the aid of a photoionization code, the ionization temperature can be determined from the nebular excitation, the luminosity of the central star can be determined from the absolute Hβ flux, and the chemical abundances can be determined from the electron temperature of the nebula and from its detailed emission-line spectrum.

Such data are available for virtually all the sample of 40 objects observed by Meatheringham and Dopita (1991), which presented the optical spectrophotometry. The absolute Hβ flux is derived from the fluxes given by Meatheringham, Dopita, and Morgan (1988), supplemented with data given in Wood, Bessell, and Dopita (1986) and Wood *et al.* (1987). A true distance modulus of $(m - M)_0 = 18.5$ is assumed for the LMC, and a modulus of $(m - M)_0 = 18.8$ is assumed for the SMC (Feast and Walker 1987). The reddening constant derived from the spectrophotometry of each object is then used in the derivation of the absolute Hβ luminosity. The local nebular density is given in Meatheringham and Dopita (1991), and is derived either from the observed [S II] 6717/6731 Å line ratio, or from the [O II] 3727/3729 Å line ratio (Dopita *et al.* 1988; Barlow 1987; Monk, Barlow, and Clegg 1988). These densities are the emission-weighted means of the particular ionization zones within which they are produced, and therefore may not be representative of other regions, or of the nebula as a whole.

We have used the generalized modeling code MAPPINGS (Binette, Dopita, and Tuohy 1985) to compute the emission-line spectra of isobaric model PN in photoionization equilibrium. The nebular gas was assumed to have a filling factor of unity in the emitting volume, but to have a shell structure with an inner radius defined by the interface between the swept-up material lost from the star during the AGB and the hot shocked stellar wind of the planetary nebular nucleus (PNn). This model is fairly well-justified by theoretical considerations, and by consideration of the observed evolutionary sequence (Dopita and Meatheringham 1990). The outer boundary is set either by the Strömgren sphere of the PNn in the case of optically thick models, or by truncation of the model at a finite optical depth at the Lyman Limit, in the case of optically thin nebulae. The pressure invariant of the models is computed in terms of the pressure that would be produced by a hydrogen plasma of a given density at a temperature of 10^4 K. Thus, to the degree to which the nebular equilibrium temperature is not dissimilar to 10^4 K, this nominal density can be thought of as the density of the model.

In these photoionization models we have assumed a blackbody photon distribution for the central star. This may yield an incorrect excitation, particularly when atmospheric blanketing in He^+ is important, as in the models of Hummer and Mihalas (1970*a*, *b*). However, we find that the blackbody approximation gives a better description of the nebular excitation than photoionization models based on the Hummer and Mihalas (1970*a*, *b*) atmospheres. In particular, the Hummer and Mihalas (1970*a*, *b*) models tend to produce [O III] line intensities which are too strong for a given overall nebular excitation, and very little change in nebular excitation occurs over the range 60,000–100,000 K as a result of the He^+ blanketing. This would produce a knot of PN on the transformed H-R diagram [i.e., the log ($F_{H\beta}$): Excitation Class plane] which is not observed (Dopita and Meatheringham 1990). The reason why blackbody models seem to work so well may lie in the fact that the stellar wind from the PNn produces an atmospheric extension which tends to reduce the blanketing effects, and restore the photon distribution towards the blackbody approximation. Indeed, Gabler *et al.* (1989) have shown that this process is very effective in a particular range of effective temperatures. At these temperatures, wind models may produce up to a thousandfold enhancement of flux shortward of the He II edge at 228 Å compared with plane-parallel atmospheric models.

b) Determination of Stellar Parameters

The emission-line spectrum of a photoionized nebula depends upon the chemical abundances, the photon energy distribution, and the ionization parameter. This parameter is defined in our case as the number of photons crossing unit area per unit time divided by the particle density, although several other equivalent definitions are possible.

The photon energy distribution determines the degree of excitation in the nebula, reflected by the excitation class (E.C.). This quantity measures the degree of ionization of helium with respect to hydrogen. However, its detailed definition differs somewhat from author to author (see Aller 1956; Feast 1968; Webster 1975; Morgan 1984). We will use here the classification given by Dopita and Meatheringham (1990), which, since it was defined in terms of two line ratios, is a continuous variable:

$$\mathrm{E.C.} = 0.45[F(5007)/F(\mathrm{H}\beta)] \qquad 0.0 < \mathrm{E.C.} < 5.0$$
$$\mathrm{E.C.} = 5.54[0.78 + F(4686)/F(\mathrm{H}\beta)] \quad 5.0 \le \mathrm{E.C.} < 10.0 .$$

In principal, such a definition is sensitive to some extent on both the chemical abundances of helium and of oxygen, and also on the ionization parameter.

We consider first the objects with E.C. > 5. In the limit of high effective temperature of the central star, the upper limit of the He II/Hβ line ratio is governed by the relative effective recombination rates. For "normal" helium abundance, viz. 0.1, this limit corresponds to about 0.7–0.8. Thus objects with an excitation class of greater than 9.0–9.5 are liable to be enhanced in helium. The excitation classification assigned to objects of lower excitation will be subject directly to the intrinsic variation of helium abundance. It is therefore preferable to use the ratio of the He II/He I lines as an indicator of the effective temperature, since this ratio is independent of both abundance effects, and of variation in the ionization parameter. In practice, the observed He I 7065 Å line intensity is very strongly affected by collisional contributions resulting from the metastable He I 2 ^3S level, which are neglected in our calculations. Other He I lines are also affected, but to a lesser extent. This problem has recently been addressed by Clegg and Harrington (1989). In order to avoid systematic errors in the determination of the effective stellar temperatures, we used the mean of the observed ratios 4686/4471, 4686/5876, and 4686/6678 Å as our temperature indicator. With these indicators, the models converge to a given effective temperature with a scatter of about ± 0.03 dex.

Let us now consider the lower excitation objects. For the case of H II regions, which, if they were PN, would be classified as having excitation classes in the range 0–2, Evans and Dopita (1985) and Dopita and Evans (1986) demonstrated that the [O III]/Hβ line ratio is sensitive to effective temperature, abundance and ionization parameter. However, most PN are objects of high ionization parameter, and for these the influence of the ionization parameter is only of second-order importance. An initial estimate of the ionization parameter can be obtained from the semiempirical evolutionary sequence of Dopita and Meatheringham (1990).

Apart from the ionization parameter, the absolute intensity of the [O III] 5007 Å line is dependent on both abundance and on the stellar temperature. The effect of increasing the abundances is to strengthen this line up to a maximum, which seems to occur at greater than solar values. Fortunately, the effect of abundance can easily be distinguished from the effect of the stellar temperature by the fact that increased abundances lead to lower electron temperatures and, therefore, weaker [O III] 4363 Å line intensities. The abundances in the model are therefore varied to produce the correct 4363/5007 Å line ratio.

With these provisos, the effective temperature of the central star can be determined primarily from the [O III] to Hβ ratio for objects in the range $0 <$ E.C. < 5. However, in view of the constancy of the Ne/O abundance ratio (Henry 1989), a very useful secondary indicator is the [Ne III] to Hβ ratio. Provided that the density is well-known so that we can allow for the effect of the collisional de-excitation of the [O II] lines, we can also use the ratio of the [O I], [O II], and [O III] lines. However, this is possible only after the effects of the $O^{++} + H^0 \rightarrow O^+ + H^+$ charge exchange reaction is taken into account (see below). Taken together, these ratios are sufficient to fix the blackbody temperature of the ionizing radiation to about ± 0.04 dex.

For the LMC abundances given by Russell and Dopita (1990) (see also Table 4), we show the general theoretical evolution of the important line intensities with changing ionization temperatures in Figure 1. This figure provides a useful first estimate of the effective temperature that is appropriate to a given object, as the results are only slightly dependent upon the mean ionization parameter.

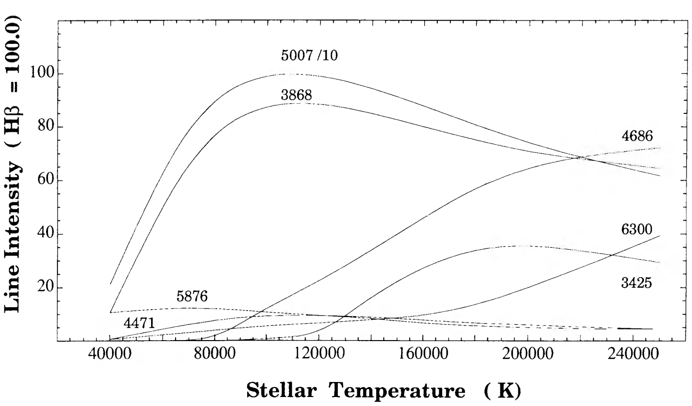

FIG. 1.—Variation of the key excitation diagnostic line intensities as a function of effective temperature of the central star for isobaric models with LMC abundances and a fixed ionization parameter of 3×10^8 cm s^{-1}. The line intensity is given in terms of the relative intensity with respect to Hβ. Note that the [O III] line 5007 Å line is scaled downward by a factor of 10.

The method of deriving effective temperature described here is closely related to the so-called energy balance method developed by Preite-Martinez and Pottasch (1983) from an original idea of Stoy (1933). This relies on the principle of thermal balance in the nebula. Hotter stars produce a greater heating effect per photoionization, and therefore a higher equilibrium temperature. However, this equilibrium temperature also depends on the nebular chemical abundances. In general, a temperature derived by a global model which allows abundance variations should be more accurate.

Given the effective temperature, the luminosity of the central star is determined by the absolute Hβ flux, in the case of optically thick objects. The luminosity was adjusted until the observed and the model line fluxes agreed. Given that the intrinsic error in the observed fluxes is about ± 0.03 dex, the error in the distance modulus is ± 0.15 dex, and the error in the reddening constant is 0.04, we estimate that derived luminosities would have a typical random error of ± 0.07 dex and a systematic error of ± 0.15 dex.

In the case of optically thin objects, it is possible to make a reasonably accurate estimate of the luminosity. This is possible because the onset of optical thinness produces an unequivocal spectral signature. Nebulae with increasing degrees of optical thinness show first a weakening and then a disappearance of the [O I] and [N I] lines, followed by a weakening of the singly ionized He, O and N species accompanied by an increase in the [O III]/Hβ and [Ne III]/Hβ line ratios. Finally, for very optically thin models, the [O III]/Hβ line ratio decreases, and the He II 4686 Å line, if initially present, increases in its relative line intensity. It is difficult to quantify the modeling errors in the determination of stellar luminosity in the case of optically thin nebulae. However, it is clear that the errors increase as the optical depth in the nebulae decreases. The additional error involved when the optical depth is as low as unity is of order ± 0.1 dex in the luminosity. However, the additional error involved in the temperature estimate is smaller, about ± 0.03 dex.

c) *Charge Exchange Reactions*

A notable problem in the modeling of PN, still outstanding, has been the attempts to predict the observed [O III]–to–[O II] line ratio 5007/3726, 9 Å (Péquignot *et al.* 1878; Che and Köppen 1983; Noriega-Crespo and McCall 1989). Our modeling is no exception, in that it predicts [O II] intensities that are stronger than observed, especially in high-excitation nebulae. This problem could be overcome by truncating the nebular model, i.e., making it optically thin. However, this would have unsatisfactory repercussions on the predicted intensities of the other low-excitation species. Che and Köppen (1983) suggest that the reason for the discrepancy lies in the Butler and Dalgarno (1980) theoretical rate of the charge-exchange reaction:

$$O^{++}(2s^2 2p^2)^3P + H(1s)^2S \rightarrow O^+(2s2p^4)^4P + H^+$$

If this had been overestimated by a factor of 10, then models and observation could be brought into accord. We find that this change has exactly the same effect on our models, and therefore was adopted for all of the modeling presented here.

The reason for an error in the theoretical rate may lie in the fact that this charge-exchange process is a two-electron process, where electron capture to a valence state is accompanied by a rearrangement of the ionic core orbitals. This process has a generally lower rate, and is more difficult to model, than the monoelectronic charge exchange (McCarroll, Valiron, and Opradolce 1983).

As far as other charge-exchange reactions are concerned, MAPPINGS includes rates for charge exchange with both He and H for all heavy elements up to Ne. To anticipate the results presented below, the fit between the modeled and observed line intensities presented in Table 1 is good enough to suggest that there are no major problems with the detailed nebular ionization structure, with one notable exception. In Table 1, the ionization balance of Ar appears to be systematically in error, in that, where Ar^{3+} exists in the nebula, the predicted [Ar IV] to [Ar III] ratio 4740/7135 Å is always much higher than observed. Taking the case of SMC 21 with a central star of effective temperature 95,000 K as a typical example. The theoretical mean ionization state has $Ar^{3+}:Ar^{2+}$ in the proportions 0.77:0.16. However, in order to correctly predict the observed line ratios, we would require $Ar^{3+}:Ar^{2+}$ in the proportions 0.55:0.35. This discrepancy is most easily explained in terms of a charge-exchange reaction which converts Ar^{3+} to Ar^{2+}.

d) The Derivation of Abundances

For a given stellar temperature, the abundances determine the electron temperature, and hence, the [O III] 4363/5007 Å line ratio. In order to have a reasonable first guess for the nebular abundances, the abundance set obtained by Russell and Dopita (1990) was initially assumed. These abundances were also derived using MAPPINGS, but applied to observations of H II regions and SNR in the Magellanic Clouds. The C/O ratio is high for PN in both our Galaxy and in the case of the small number of non-type I objects so far studied in the ultraviolet with *IUE* (Aller *et al.* 1987). For type I objects, the C/O ratio is low, reflecting the differences in burning and dredge-up. For the purposes of modeling, we assumed a typical C/O ratio of 1.5, recognizing that individual objects may differ appreciably from this figure. However, errors in this quantity have only a second order impact on the derived abundances.

The overall nebular abundances, the luminosity, and the temperature of the central star were iterated as described above until the nebular flux, excitation, and temperatures agreed, within the errors, with the photoionization models. The pressure parameter is determined by forcing agreement between the predicted and observed [S II] and [O II] densities. When the parameters of the photoionization model all agree, within the errors of observation and modeling, with the observed parameters of the PN, the abundances of N, S, Ne, and Ar are fine-tuned to give the best agreement with observation. This point is typically reached after five iterations.

IV. RESULTS

A comparison of the observed and predicted line ratios for all the 38 PN modeled is not very instructive, so in Table 1 we show this comparison for selected PN which, taken together, cover the full range of parameter space for which we have observations. The first three objects, LMC 5, 63, and 15, represent, respectively, a low-, medium- and high-excitation non-type I PN. LMC 58 is chosen because it is the densest object in the sample which has been modeled, LMC 96 is an extreme type I object, and LMC 76 is an optically thin PN.

Despite the wide range of nebular and stellar parameters represented in Table 1, the agreement between the model and the observations is generally excellent. The notable exceptions to this agreement are as follows: first, the model [Ar III] and [Ar IV] relative intensities are in poor agreement with observa-

TABLE 1

COMPARISON OF THE OBSERVED AND MODELED RELATIVE LINE INTENSITIES FOR SOME LMC PN

		OBSERVATION MODEL											
λ (Å)	IDENTIFICATION	SMP 05		SMP 63		SMP 15		SMP 58		SMP 96		SMP 76	
3426	[Ne V]	...	...	...	...	2	...	...	...	45	39	...	...
3727	[O II]	225	163	32	37	21	21	8	12	176	128	22	19
3868	[Ne III]	5	5	58	55	101	96	30	33	120	157	34	48
3967, 70	[Ne III], H7	27	18	30	33	46	45	25	25	58	64	31	31
4069, 76	[S II]	...	1	2	2	4	3	...	1	...	12	2	...
4101	Hδ	27	26	26	26	28	26	26	26	26	25	26	26
4340	Hγ	46	47	46	47	46	47	47	47	48	46	46	47
4363	[O III]	4	3	10	12	16	17	9	10	27	13	5	5
4471	He I	4	4	6	6	4	4	6	5	...	5	5	4
4686	He II	...	...	...	1	31	31	2	1	91	91	...	...
4740	[Ar IV]	...	...	2	6	2	8	...	2	4	9	...	7
4861	Hβ	100	100	100	100	100	100	100	100	100	100	100	100
4959	[O III]	95	102	339	330	343	360	244	261	224	199	201	210
5007	[O III]	270	293	966	950	1040	1040	714	750	644	574	578	606
5199	[N I]	...	...	...	...	...	...	...	...	6	62	...	...
5876	He I	10	10	14	16	18	10	13	14	18	13	15	12
6300	[O I]	...	1	2	3	12	7	2	2	27	22	...	...
6312	[S III]	...	1	1	3	...	5	2	3	7	9	...	2
6548	[N II]	4	4	6	6	10	11	2	3	206	201	3	3
6563	Hα	270	283	280	282	285	285	285	282	273	309	280	283
6584	[N II]	13	13	18	17	30	32	6	9	603	607	10	9
6678	He I	2	3	5	5	3	3	3	4	4	4	3	...
6717	[S II]	...	2	2	2	4	4	...	...	50	46	...	...
6731	[S II]	...	3	3	3	7	8	...	...	60	59	...	...
7005	[Ar V]	...	...	...	...	...	4	...	...	11	6	...	...
7135	[Ar III]	3	3	16	5	12	5	8	4	30	16	6	10
7320	[O II]	3	5	10	4	8	4	7	7	13	5	...	2
7330	[O II]	4	4	6	3	5	3	7	5	10	4	...	2

tion, a problem which we have already discussed and ascribed to a charge exchange reaction. Second, the predicted [N I] line intensity is far too strong in the case of type I objects. Third, the [O III] intensity ratio 4363/5007 Å is in poor agreement with observation in the case of the type I objects. This problem can be alleviated somewhat by lowering the abundance of carbon, but even so, the extreme [O III] temperatures which we observed in some type I objects cannot be reproduced. Models of type I PN also display another problem. In some cases, we strongly underestimate the strength of the [Ne V] line in models.

It is not surprising that these simple models have problems with the type I objects. Galactic examples of type I PN usually show a complex, filamentary, bipolar structure with an embedded dust ring. This geometrical structure bears no relationship to our spherical shell model, and a more complex ionization model should be adopted (e.g., Clegg *et al.* 1987). A second reason for failure of the models is that in type I PN, winds play an important role in determining nebular morphology (Meaburn and Walsh 1980; Barral *et al.* 1982; Lopez and Meaburn 1983; Webster 1978). These may be seen as broad high-velocity wings on the [Ne V] lines, and they probably contribute directly to nebular heating in the inner regions (Harrington 1989). This is the probable cause of both the strong [Ne V] lines and the extreme [O III] temperatures.

a) Parameters of the Central Stars

The effective temperature and luminosities of the central stars, as derived from the modeling, are given in Table 2. This list more than doubles the sample of Magellanic Cloud PNn which have been placed on the Hertzsprung-Russell diagram, previous studies being those of Aller *et al.* (1987) and Monk, Barlow, and Clegg (1988).

The Aller *et al.* (1987) work refers to eight high-excitation PN for which the central star cannot be detected, even with *IUE*. It therefore relied on a detailed photoionization model, in a similar fashion to that used in this paper. The Monk, Barlow, and Clegg (1988) study used a sophisticated best-fit analysis of model stellar atmospheres to the results of both the hydrogen Zanstra and Stoy energy-balance methods. This was applied to

TABLE 2

PARAMETERS OF THE PLANETARY NEBULAE AS DETERMINED FROM THE NEBULAR MODELS

Object	L_* ($L_\odot$)	T_{eff} (K)	$P/10^4$ (cm^{-3} K)	R_{in} (pc)	R_{out} (pc)	M_{neb} ($M_\odot$)	τ_{out} (H)
			LMC				
SMP 01	7000	66,000	3700	0.065	0.102	0.406	2.800
SMP 05	8775	43,000	1850	0.032	0.185	1.387	
SMP 06	8250	150,000	16000	0.032	0.055	0.214	
SMP 08	5575	53,000	5500	0.084	0.090	0.109	1.500
SMP 15	6790	135,000	6000	0.065	0.100	0.471	
SMP 20	1190	205,000	1800	0.010	0.112	0.286	
SMP 23	3950	65,000	5200	0.042	0.063	0.113	2.000
SMP 37	3360	155,000	9250	0.013	0.054	0.151	
SMP 47	4090	150,000	5400	0.010	0.076	0.302	
SMP 50	2400	100,000	8400	0.023	0.053	0.139	
SMP 52	4990	125,000	3300	0.023	0.097	0.466	
SMP 55	4360	39,000	18000	0.032	0.038	0.052	
SMP 56	1500	42,000	3000	0.013	0.066	0.097	3.000
SMP 58	5790	63,000	76000	0.019	0.022	0.029	
SMP 60	1600	195,000	1500	0.032	0.108	0.158	5.500
SMP 61	3995	59,000	8000	0.045	0.063	0.181	
SMP 63	4160	82,000	9000	0.023	0.058	0.212	
SMP 65	1215	60,000	14500	0.019	0.024	0.012	2.000
SMP 67	1940	46,000	3800	0.032	0.062	0.127	
SMP 76	8000	50,000	15000	0.026	0.041	0.095	3.000
SMP 77	2640	46,000	3600	0.032	0.079	0.238	
SMP 83	2880	170,000	2880	0.016	0.126	0.631	
SMP 85	6150	43,000	23000	0.016	0.029	0.066	
SMP 88	4660	230,000	6000	0.013	0.111	0.575	
SMP 89	8560	99,000	5400	0.065	0.113	0.751	
SMP 96	945	250,000	3000	0.010	0.071	0.134	
SMP 97	6000	175,000	2500	0.032	0.136	0.541	8.000
			SMC				
SMP 01	2930	41,000	11000	0.026	0.042	0.071	
SMP 03	2400	92,000	2400	0.036	0.090	0.181	2.000
SMP 07/J 1	350	98,000	3000	0.006	0.074	0.088	7.000
SMP 13	5240	84,000	2150	0.039	0.175	1.308	
SMP 15	4360	58,000	60000	0.013	0.019	0.033	
SMP 16	11200	37,000	14400	0.042	0.057	0.179	
SMP 21	1750	95,000	15000	0.010	0.035	0.073	
SMP 22	2740	220,000	4000	0.036	0.114	0.577	
SMP 22	2740	200,000	5000	0.026	0.082	0.274	
SMP 25	1045	170,000	1700	0.006	0.075	0.200	
SMP 26	1800	180,000	5500	0.016	0.120	0.313	
MG 1	810	200,000	2000	0.016	0.069	0.050	1.700

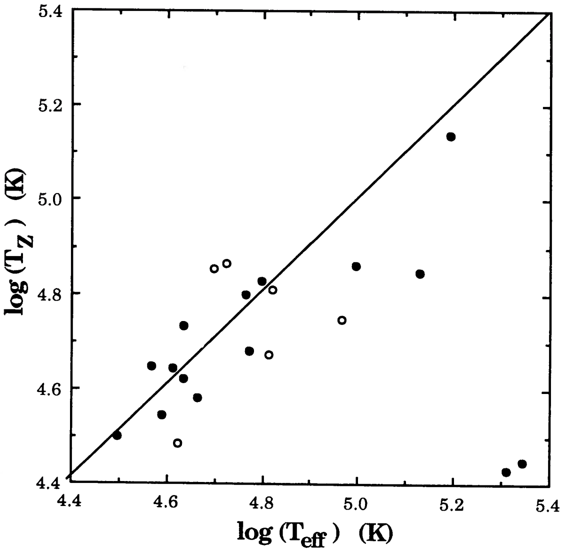

FIG. 2.—Correlation between the excitation balance temperature and the Zanstra temperature for objects in which both are measured. We also include the point for LMC SMP 64, reported elsewhere (Dopita and Meatheringham 1991*a*).

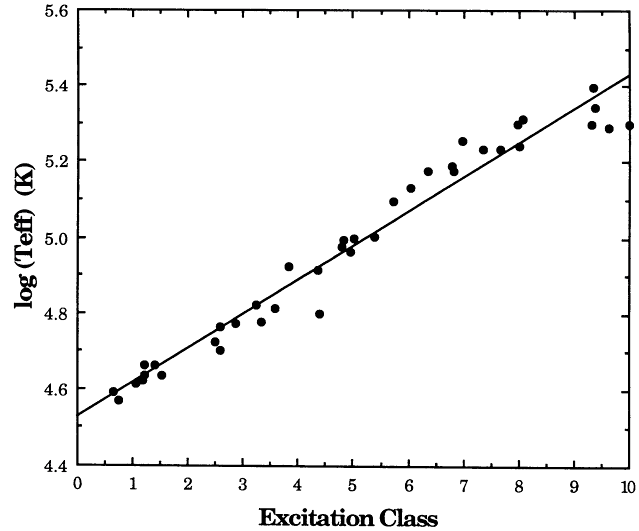

FIG. 3.—Correlation between excitation class as defined in the text, and the excitation balance temperature derived from models.

nine objects of generally lower effective temperature than the Aller *et al.* (1987) sample.

An instructive test of the validity of the excitation balance temperatures derived here, is the comparison of these with the Zanstra-temperatures obtained earlier (Meatheringham and Dopita 1991). This is shown in Figure 2 and includes the extreme low-temperature object LMC 64 modeled elsewhere (Dopita and Meatheringham 1991*a*). Objects which require optically thin models are shown as open circles. In the cases of LMC 20 and LMC 88, the Zanstra temperature gives a very low value compared with the excitation balance temperature. These objects also show a Zanstra discrepancy in that the helium Zanstra temperature is much higher, but still less than the excitation balance temperature. Both objects are type I PN. With such a gross disagreement between the various methods of deriving the temperature, we are forced to conclude that either the central star is a binary, or else another star lies by chance along the line of sight to the nebula. Excluding these two objects, there is a good correlation between the two techniques at low temperatures, but at the highest temperatures there may be some evidence for a Zanstra discrepancy. More observations would be required to be certain of this.

The excitation class (E.C.), as defined earlier, turns out to give an excellent measure of the excitation balance temperature (see Fig. 3). The correlation between E.C. and log (T_{eff}) is linear, with a correlation coefficient of 0.96.

The Hertzsprung-Russell (H-R) diagram resulting from our analysis is shown in Figure 4, where the optically thick, optically thin and type I PN are distinguished by separate symbols. Given the smallness of our sample, we do not distinguish between the LMC and SMC objects in this paper, since the populations of PN in the two systems are quite similar. We leave the discussion of the comparison of the populations in the two Clouds to a future paper (Dopita and Meatheringham 1991*b*, in preparation). The optically thick objects are found in a range of core masses between 0.56–0.70 $M_\odot$, with a mean of about 0.62 $M_\odot$. This is consistent with the results of Barlow (1989), or Dopita and Meatheringham (1990). However, it is very evident that the mean mass is higher, and the range of core masses wider, than those derived by Schönberner (1981) for a group of nearby, evolved PNn. Despite our efforts to select the PN to be observed throughout the range of flux, density, and excitation class, our sample still suffers from selection effects, since the faintest PN will tend to be missed. Furthermore, the rate of evolution across the H-R diagram is expected to be very high in the case of the

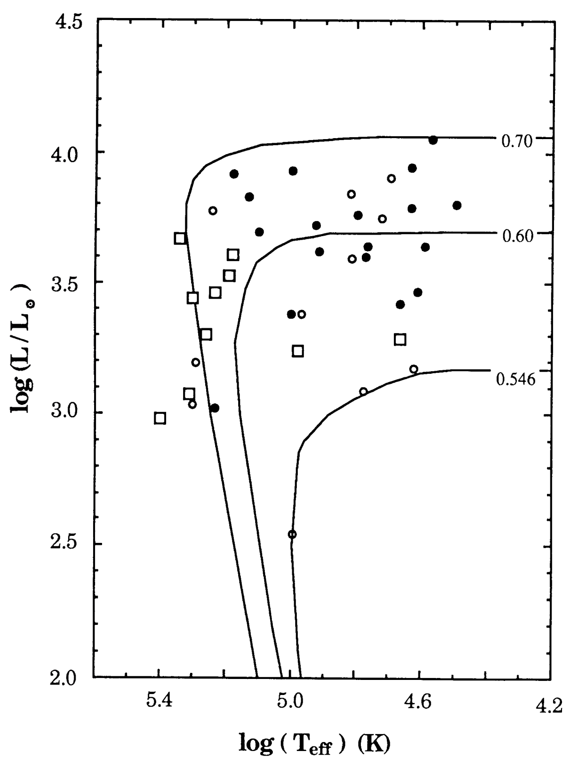

FIG. 4.—Hertzsprung-Russell Diagram for the Magellanic Cloud PN. The evolutionary tracks for different core masses are from Schönberner (1981) and Wood and Faulkner (1986). The open circles represent optically thin objects, the filled circles optically thick PN and the open squares are type I planetaries. The type I objects tend to be objects of higher core mass, up to 1.0 $M_\odot$.

more massive PNn. Allowing for these effects is difficult, and depends upon assumptions on the IMF and the age distribution of the stellar precursors (Shaw 1989). However, it is clear that both selection and evolutionary effects will tend to broaden the true mass range of PNn still further.

Note that the type I PN are found preferentially at high $T_{\rm eff}$ and, in general, at larger values of the core mass. This is consistent with the type I PN representing the more massive progenitor stars, and therefore, as a result of their rapid evolution across the diagram, are preferentially found on the descending portions of the evolutionary tracks. The object with the most massive core, LMC 96, is also the most extreme type I object in the sample, and appears to have a core mass of about 1.0 $M_\odot$.

The optically thin PN occupy a broad region of the diagram, but of somewhat lower mean mass, from 0.546–0.65 $M_\odot$. Note that the three objects lying on the 0.546 $M_\odot$ track are all optically thin objects. These PN, LMC 56, LMC 65, and SMC 7 (J I), also have low nebular masses; 0.097, 0.012, and 0.88 $M_\odot$, respectively. This implies that the efficiency of mass-loss during the AGB is a very strongly decreasing function of the core mass and luminosity, since at the tip of the AGB, these are related through the formula (Wood and Zarro 1981);

$$L/L_\odot = 59250(M_c/M_\odot - 0.495) .$$

Note that, apart from type I PN, very few objects are observed on the descending portions of the evolutionary tracks. This is simply a selection effect resulting from use of a magnitude-limited sample. The Jacoby objects observed by Henry, Leibert, and Boroson (1989) are concentrated in this evolutionary phase. In future papers, we will present data on the Morgan and Good (1985) sample, and on the new Morgan (1990) sample, which will rectify this omission.

b) Nebular Paraameters

The results of the nebular parameters are given in Table 2. The inner radius, $R_{\rm in}$, represents the boundary between the swept-up photoionized gas and the hot shocked stellar wind, and is not very well-determined. If it is made too large, the ionization parameter falls too low, and lines of low ionization degree becomes too strong. The observations require an ionization parameter typically in the range $3 \times 10^8 > \langle Q \rangle > 10^8$ cm s^{-1}, so, with a given nebular pressure parameter, this determines the inner radius to an accuracy of about a factor of 2. The nebular pressure parameter P is chosen to give best agreement with the [O II] and [S II] densities. With a given luminosity, density, pressure parameter, and hydrogen optical depth, $\tau_{\rm out}$, the outer radius, $R_{\rm out}$, is then determined. The models return the mean hydrogen particle density in the nebula. The total mass of the nebula is derived from this quantity via the formula

$$M_{\rm neb} = (4/3)\pi(R_{\rm out}^3 - R_{\rm in}^3) m_{\rm H} N_{\rm H}[1 + 4Z({\rm He})] ,$$

where $m_{\rm H}$ is the mass of the hydrogen atom, and Z(He) is the abundance of helium, by number with respect to hydrogen. Note that the uncertainty in $R_{\rm in}$ has little effect on the accuracy of the result.

Gathier *et al.* (1983) and, more recently, Pottasch and Acker (1989) have pointed out the strong relationship between nebular mass and nebular radius. They argue, as have Dopita and Meatheringham (1990), that this relationship is strong evidence in support of the idea that the majority of these PN are optically thick. Here, we turn this argument around, and look at the mass:radius relationship for only those nebulae which the photoionization analysis shows are optically thick. The result shown in Figure 5 reveals a remarkably tight log R:log M correlation with a slope of 1.7 ± 0.2. Inclusion of the optically thin objects produces a scattering of points below the lines, as would be expected. However, the remarkable thing is that optically thin nebulae are found even for PN of small radius having relatively unevolved central stars of low effective temperature (e.g., LMC SMP 8, LMC SMP 65). This reinforces our conclusion that the intrinsic scatter in the wind parameters during the AGB phase of evolution is quite large.

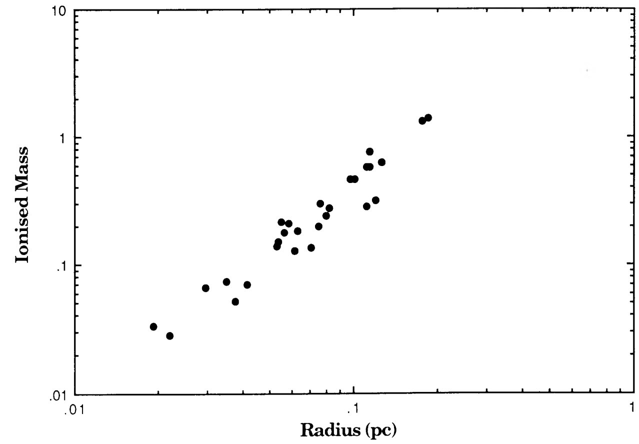

FIG. 5.—Correlation between the nebular mass and radius for the optically thick objects in the sample. Note the existence of PN with nebular masses in excess of 1.0 $M_\odot$. The optically thin objects lie to the right, and below, of this correlation.

What is also surprising is the presence of two high-mass optically thick PN, LMC SMP 5 and SMC SMP 13, each with nebular masses in excess of 1.0 $M_\odot$. As the nebula expands to lower density, it can ionize a greater mass for a given luminosity of the central star. Thus, we would expect that the low-density/high-mass PN have a greater fraction of optically thin PN amongst them. The results of Dopita and Meatheringham (1990) suggest that the optically thick/thin transition lies at a nebular mass of about 0.5 $M_\odot$. However, the detailed models presented here show no evidence for such a transition. High-mass PN have also been found in the Galactic Center sample (Pottasch and Acker 1989), and it is likely that these objects are derived from higher mass progenitors.

In view of the correlation between E.C. and $T_{\rm eff}$, it is not surprising that the effective temperature and the velocity of expansion are fairly well-correlated (see Fig. 6), since such a correlation has been earlier discovered between E.C. and velocity of expansion (Dopita *et al.* 1985). A better correlation was found in a two-parameter fit of E.C. and Hβ flux with the expansion velocity (Dopita *et al.* 1987; Dopita and Meatheringham 1990). Since the Hβ flux scales closely with the luminosity of the central star, for optically thick objects, we have rederived this fit in terms of Hertzsprung-Russell diagram parameters; log $T_{\rm eff}$ and log $(L/L_\odot)$:

$$(V_{\rm eff}/{\rm km\ s^{-1}}) = -(128 \pm 4) + (38 \pm 2)[\log (T_{\rm eff}) - (0.25 \pm 0.05) \log (L/L_\odot)]$$

The result of this fitting formula is compared with the observed velocity of expansion in Figure 7. The correlation coefficient is 0.7. It is clear that this relationship is fundamental

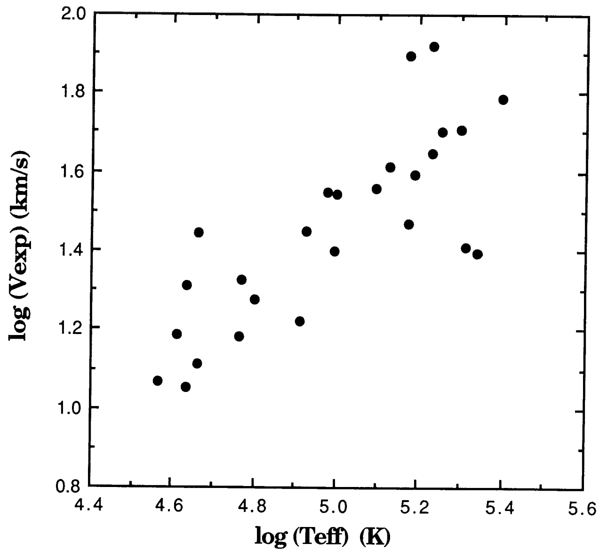

FIG. 6.—Correlation between the expansion velocity of the nebula and the effective temperature of the central star.

to the understanding of the dynamical evolution of PN. Curiously enough, there is little or no correlation of the dynamical age (R_{neb}/V_{exp}) with the effective temperature. This forces the conclusion that the dynamical age is not a measure of the true age. Such a situation can arise in an accelerated nebula if the velocity of expansion is correlated with the nebular radius, which is true, but with a very large scatter, for our sample. This once again demonstrates that nebular shells are accelerated during the evolution of the PNn towards higher temperatures (see Dopita and Meatheringham 1990).

c) *Nebular Abundances*

Table 3 gives the chemical abundances derived for the sample. For helium, our models include only recombination processes, the effect of optical depth in the Lyman series, and the effect of collisions from the ground state in the population of any given level. In fact, it has recently become clear that a more complex treatment is required for He I, which takes account of collisional excitation and ionization from excited states. Inclusion of these would cause a downward correction in the abundances derived, according to the formulation of Clegg and Harrington (1989). This has not been done here, since we are in the process of inclusion of these additional processes in the models, and until this is completed, we are uncertain of the exact size of this correction in individual objects. To minimize errors due to this cause, we have derived the mean He^+ abundance using the 4471, 5876, and 6678 Å lines, which are not seriously affected by the metastability of the 2^3S level. We therefore expect that errors in derived abundances are reduced to $<10\%$. However, this problem should be borne in mind in the discussion which follows.

The Argon abundances have been empirically corrected, taking into account the difference between the observations and the models, as far as the relative Ar III/Ar IV ratios are concerned.

An important test of the modeling is to see to what extent the derived nebular abundances are dependent upon nebular conditions. If these show a wide variation, it would suggest that the models are not an accurate representation of reality, and that errors in modeling the ionization structure are producing unreliable abundances. However, it is important to choose a more homogeneous subsample to test, by eliminating the type I PN which are affected by dredge-up processes and consequently display a real spread in abundances, particularly in the case of nitrogen. We have already shown that the type I objects are concentrated in the high-temperature portion of the H-R diagram. We somewhat arbitrarily take the division between type I and "normal" PN to be at a derived N/O ratio of 0.3. This having been done, we show in Figure 8 the variation of the estimated abundance of the principal coolants with effective stellar temperature for the LMC PN. Oxygen, the key coolant, shows very little variation, and very little scatter,

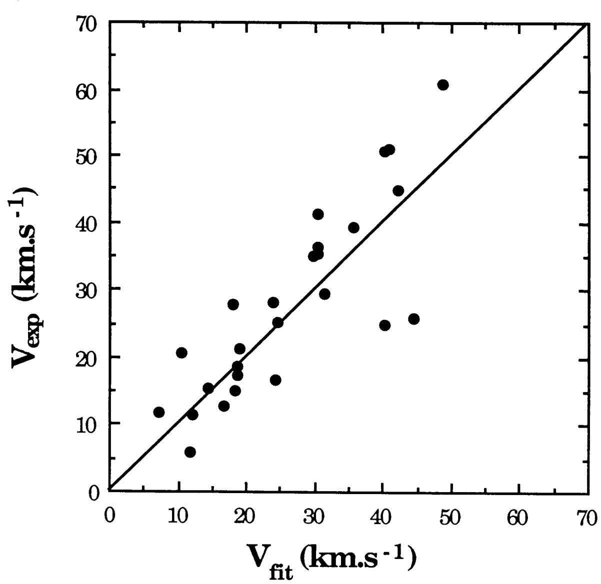

FIG. 7.—Correlation between the expansion velocity of the nebula, and that estimated from a two-parameter fit involving the H-R diagram parameters of the central star; log T_{eff} and log ($L/L_{\odot}$).

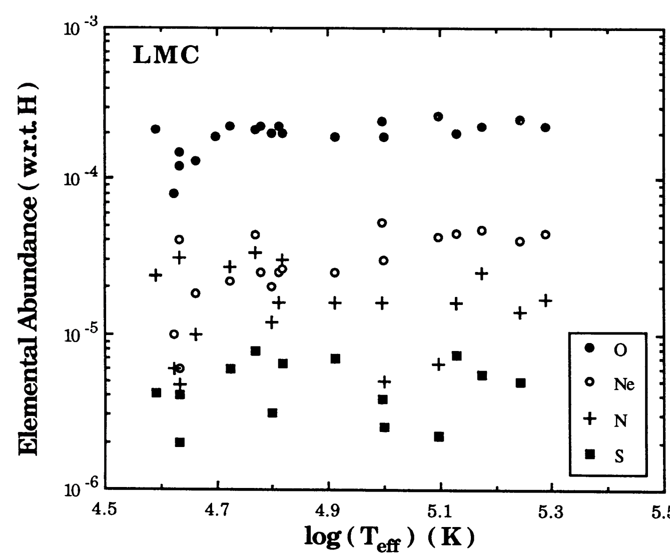

FIG. 8.—Variation of chemical abundances with the effective temperature of the central star as derived from the models for optically thin and optically thick non-type I nebulae. The absence of any marked trend can be taken as proof that the unseen unionization stages are being correctly taken into account.

except for three low-temperature PN, which are low in oxygen, but which also show depletions in other elements, and are therefore genuine low abundance objects. There is very little trend visible in any of the other elemental abundances. We conclude that the models are not affected in any major way by unseen ionization stages, and the associated implicit ionization correction factors.

The mean abundances, derived without consideration of the type I planetaries, which are known to be helium- and nitrogen-enriched, is given in Table 4. We also compare these abundances with some previously published estimates for PN , H II regions, and evolved SNR (Aller *et al.* 1987; Dufour, Shields, and Talbot 1982; Monk, Barlow, and Clegg 1988; Russell and Dopita 1990). It is a striking result that all the abundances with some previously published estimates for PN, H II regions, and evolved SNR (Aller *et al.* 1987; Dufour, the Magellanic Clouds. This estimate was based on spectrophotometry of a similar standard, and upon analysis using MAPPINGS.

Our results for nitrogen are quite different from the results of Aller *et al.* (1987) and Monk, Barlow, and Clegg (1988). Only part of this difference can be ascribed to the fact that we rejected the type I objects from the mean, and therefore this discrepancy is not fully understood.

The difference between the type I objects and the sample as a whole is clearly exemplified in Figure 9, in which we plot the N/O ratio as a function of helium abundance. Note that many points are found around the mean points for the LMC and the SMC found by Russell and Dopita (1990), and the type I objects stand out as having both high He/H ratios and high N/O ratios. Such a diagram has been extensively used by Kaler (1983, 1985) as a diagnostic of the importance of the various dredge-up processes occurring during the giant and AGB phase of evolution (Becker and Iben 1980; Renzini and Voli 1981). The first of these occurs during the giant branch evolution when the convective envelope dips into the nuclear-burning shell. This increases the N/O ratio, but produces little change in He. In the second, occurring in AGB stars with

TABLE 3

CHEMICAL ABUNDANCES OF THE PLANETARY NEBULAE DETERMINED FROM NEBULAR MODELS

Object	Chemical Abundances (by Number with Respect to Hydrogen)					
	He	N	O	Ne	S	Ar
LMC						
SMP 01	0.146	3.0E−5	2.0E−4	2.6E−5	6.5E−6	1.0E−6
SMP 05	0.082	4.8E−6	1.2E−4	6.0E−6	2.0E−6	3.0E−7
SMP 06	0.107	2.5E−5	2.2E−4	4.7E−5	5.6E−6	1.3E−6
SMP 08	0.100	2.7E−5	2.2E−4	2.2E−5	6.0E−6	1.4E−6
SMP 15	0.099	1.6E−5	2.0E−4	4.4E−5	7.5E−6	1.1E−6
SMP 20	0.130	1.2E−4	1.5E−4	7.7E−5	7.3E−6	2.7E−6
SMP 23	0.095	1.6E−5	2.2E−4	2.5E−5		1.8E−6
SMP 37	0.110	9.0E−5	2.2E−4	4.1E−5	6.8E−6	1.6E−6
SMP 47	0.162	1.5E−4	2.4E−4	7.6E−5	6.8E−6	2.7E−6
SMP 50	0.120	5.0E−6	1.9E−4	3.0E−5	2.5E−6	4.6E−7
SMP 52	0.090	6.5E−6	2.6E−4	4.2E−5	2.2E−6	1.4E−6
SMP 55	0.110	2.4E−5	2.1E−4		4.2E−6	9.0E−7
SMP 56	0.091	6.0E−6	8.0E−5	1.0E−5		6.0E−7
SMP 58	0.105	1.2E−5	2.0E−4	2.0E−5	3.1E−6	5.0E−7
SMP 60	0.091	1.7E−5	2.2E−4	4.5E−5		
SMP 61	0.140	3.3E−5	2.1E−4	4.3E−5	7.8E−6	1.7E−6
SMP 63	0.125	1.6E−5	1.9E−4	2.5E−5	7.0E−6	1.1E−6
SMP 65	0.110		2.2E−4	2.5E−5		
SMP 67	0.139	1.1E−4	2.0E−4	4.0E−5	5.7E−6	1.4E−6
SMP 76	0.091		1.9E−4			7.0E−7
SMP 77	0.135	1.0E−5	1.3E−4	1.8E−5		7.0E−7
SMP 83	0.137	4.5E−5	1.8E−4	4.1E−5	6.5E−6	2.4E−6
SMP 85	0.104	3.1E−5	1.5E−4	4.0E−5	4.0E−6	7.7E−7
SMP 88	0.170	3.3E−5	6.0E−5	2.0E−5	2.0E−6	2.0E−6
SMP 89	0.115	1.6E−5	2.4E−4	5.2E−5	3.8E−6	8.8E−7
SMP 96	0.175	1.6E−4	1.3E−4	5.7E−5	1.1E−5	3.0E−6
SMP 97	0.091	1.4E−5	2.5E−4	4.0E−5	5.0E−6	1.8E−6
SMC						
SMP 01	0.080	5.6E−6	1.4E−4	7.0E−6		4.2E−7
SMP 03	0.130	1.9E−5	1.1E−4	1.2E−5		6.0E−7
SMP 07/J 1	0.080	8.0E−6	1.4E−4	2.6E−5	6.0E−6	6.0E−7
SMP 13	0.112	2.9E−6	1.4E−4	1.7E−5	1.4E−6	3.0E−7
SMP 15	0.109	5.0E−6	1.2E−4	2.1E−5		4.0E−7
SMP 16	0.075	3.5E−6	1.2E−4	1.0E−5	2.0E−6	2.0E−7
SMP 21	0.160	5.7E−5	1.0E−4	1.8E−5		1.2E−6
SMP 22	0.135	7.0E−5	6.0E−5	2.2E−5	3.0E−6	8.0E−7
SMP 22	0.141	6.0E−5	7.0E−5	2.0E−5	3.5E−6	3.6E−7
SMP 25	0.080					
SMP 26	0.120	7.3E−5	1.1E−4	2.6E−5	2.5E−6	7.4E−7
MG1	0.130		1.0E−4	2.0E−5		

TABLE 4

MEAN CHEMICAL ABUNDANCES IN THE MAGELLANIC CLOUDS

Galaxy	Reference	He/H[a] (by number)	Abundances: 12 + log [$N(i)/N$(H)]				
			N	O	Ne	S	Ar
LMC	PN: This work	0.106[a]	7.23 ± 0.20	8.30 ± 0.06	7.52 ± 0.13	6.67 ± 0.15	6.00 ± 0.25
	H II, SNR: RD	0.091	7.14 ± 0.18	8.35 ± 0.06	7.61 ± 0.05	6.81 ± 0.09	6.29 ± 0.25
	PN: MBC	0.105[a]	7.81 ± 0.30	8.49 ± 0.15	7.64 ± 0.19		
	PN: Aller *et al.* 87		7.56 ± 0.31	8.28 ± 0.11	7.50 ± 0.13		
	H II: DST 82	0.083	6.97 ± 0.10	8.43 ± 0.08	7.64 ± 0.10	6.85 ± 0.11	6.20 ± 0.06
SMC	PN: This work	0.100[a]	6.74 ± 0.24	8.08 ± 0.08	7.23 ± 0.15	6.43 ± 0.20	5.60 ± 0.25
	H II, SNR: RD	0.081	6.63 ± 0.20	8.03 ± 0.10	7.27 ± 0.20	6.59 ± 0.15	5.81 ± 0.08
	PN: MBC	0.083[a]	7.44 ± 0.28	8.26 ± 0.15	7.36 ± 0.22		
	PN: Aller *et al.* 87		7.42 ± 0.22	8.16 ± 0.12	7.46 ± 0.27		
	H II: DST 82	0.083	6.46 ± 0.12	8.02 ± 0.08	7.22 ± 0.12	6.49 ± 0.14	5.78 ± 0.12

[a] The helium abundances are given neglecting the collisional effects in He I. For the correction for these effects, see Barlow 1989.

References.—(RD) Russell and Dopita 1990; (MBC) Monk, Barlow, and Clegg 1988; (Aller *et al.* 87) Aller *et al.* 1987; (DST 82) Dufour, Shields, and Talbot 1982.

$M > 3\ M_\odot$, both N and He are dredged up. The third phase takes place during the thermal pulsing phase of the AGB, and increases C/O and He/H at the expense of the N/O ratio. However, the so-called "hot bottom burning" can convert C to N, and so produce very large N/O ratios in the PN. Kaler (1983, 1985) concludes that the observational data do not support the hypothesis of "hot bottom burning" and dredge-up, since this gives too much N. However, if the third dredge-up phase occurs, some conversion of C to N must occur, although at about the maximum rate allowed by theory.

In Figure 9 we also show the approximate enrichment path according to this scenario. Note the existence of "transition" type I objects in the region He/H < 0.11. Clearly the Magellanic Cloud sample yields a similar result to the Galactic sample of Kaler (1983, 1985). We too find some very large He abundances which are not easily accounted for by theory, but no objects as extreme as some of those in the Galactic sample. The

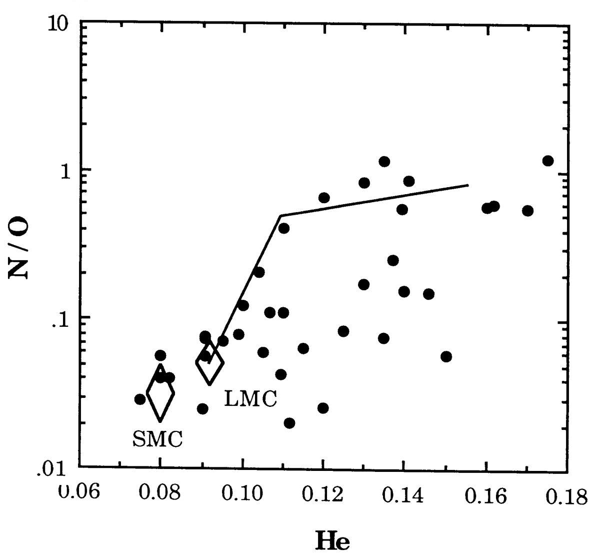

FIG. 9.—Variation of N/O with He/H for nebulae in both the SMC and the LMC. The error diamonds represent the mean abundance ratios for the SMC and the LMC derived from observation of H II regions and SNR by Russell and Dopita (1990). The line is for an enrichment scenario in which the third dredge-up occurs, but in which C is converted to N at half of the maximum rate. This could account for the type I objects.

lower initial N/O ratios improve discrimination between the various enrichment scenarios. It is apparent from Figure 9 that some objects show appreciable He enhancements without any corresponding N/O enhancement. Indeed, for objects with He/H > 0.11, the sample has a completely bimodal character in which the type I objects appear in the range 0.4 < N/O < 1.3, and the rest are concentrated in the zone N/O < 0.3. This is a signature of the third dredge-up phase without C to N conversion. Since the type I objects have been shown to have more massive core masses, and hence more massive precursors, we can conclude that the C/N conversion is mass-dependent. This conclusion will be shortly tested by HST observations of the C/O ratio.

V. CONCLUSIONS

The self-consistent photoionization modeling of a first sample of 38 Magellanic Cloud Planetary Nebulae (PN) has allowed us to construct a Hertzsprung-Russell (H-R) Diagram for the central stars, and has given both the nebular chemical abundances and the physical parameters of the nebulae. This allows us to reach the following conclusions:

1. Effective temperatures, $T_{\rm eff}$, derived from nebular excitation analysis are in agreement with the temperatures derived by the classical Zanstra method.

2. There is a linear correlation between log ($T_{\rm eff}$) and the excitation class.

3. The majority of the central stars in this sample with optically thick nebulae have masses between 0.55 and 0.7 $M_\odot$ and are observed during their hydrogen-burning excursion towards high temperatures.

4. Optically thin objects are found scattered throughout the H-R diagram, but tend to have a somewhat smaller mean mass.

5. The type I PN are found to have high core masses and to lie on the descending branch of the evolutionary tracks. The highest mass PNn are therefore likely to have been missed in this flux-limited sample. The type I objects show evidence for a third dredge-up episode resulting in correlated He and N abundance enhancements.

6. The nebular mass of the optically thick objects is closely related with the nebular radius, and PN with nebular masses in excess of 1 $M_\odot$ are observed.

7. The velocity of expansion of the nebula is very well-

correlated with the position of the central star on the H-R diagram, and is evidence of continual acceleration of the nebular shell during the transition toward high effective temperatures.

8. Excluding the type I PN, the mean abundances derived for the LMC and the SMC agree very well with the mean abundances previously derived from observation of the H II regions and evolved radiative supernova remnants.

REFERENCES

Abbot, D. C. 1978, *Ap. J.*, **225**, 893.
Aller, L. H. 1956, *Gaseous Nebulae* (New York: Wiley).
———. 1983, *Ap. J.*, **273**, 590.
Aller, L. H., Keyes, C. D., Maran, S. P., Gull, T. R., Michalitsianos, A. G., and Stecher, T. P. 1987, *Ap. J.*, **320**, 159.
Aller, L. H., Keyes, C. D., Ross, J. E., and O'Mara, B. J. 1981, *M.N.R.A.S.*, **194**, 613.
Barlow, M. J. 1987, *M.N.R.A.S.*, **227**, 161.
———. 1989, in *IAU Symposium No. 131, Planetary Nebulae*, ed. S. Torres-Peimbert (Dordrecht: Kluwer), p. 319.
Barral, J. F., Canto, J., Meaburn, J., and Walsh, J. R. 1982, *M.N.R.A.S.*, **199**, 817.
Becker, S. A., and Ibsen, I., Jr. 1980, *Ap. J.*, **237**, 111.
Binette, L., Dopita, M. A., and Tuohy, I. R. 1985, *Ap. J.*, **297**, 476.
Butler, S. E., and Dalgarno, A. 1980, *Ap. J.*, **241**, 838.
Che, A., and Köppen, J. 1983, *Astr. Ap.*, **118**, 107.
Clegg, R. E. S., and Harrington, J. P. 1989, *M.N.R.A.S.*, **239**, 869.
Clegg, R. E. S., Harrington, J. P., Barlow, M. J., and Walsh, J. R. 1987, *Ap. J.*, **314**, 551.
Dopita, M. A., and Evans, I. N. 1986, *Ap. J.*, **307**, 431.
Dopita, M. A., Ford, H. C., Lawrence, C. J., and Webster, B. L. 1985, *Ap. J.*, **296**, 390.
Dopita, M. A., Ford, H. C., and Webster, B. L. 1985, *Ap. J.*, **297**, 593.
Dopita, M. A., and Meatheringham, S. J. 1990, *Ap. J.*, **357**, 140.
———. 1991*a*, *Ap. J. (Letters)*, submitted.
———. 1991*b*, *Ap. J.*, submitted.
Dopita, M. A., Meatheringham, S. J., Webster, B. L., and Ford, H. C. 1988, *Ap. J.*, **327**, 639.
Dopita, M. A., Meatheringham, S. J., Wood, P. R., Webster, B. L., Morgan, D. H., and Ford, H. C. 1987, *Ap. J. (Letters)*, **315**, L107.
Dufour, R. J., Shields, G. A., and Talbot, R. J. 1982, *Ap. J.*, **252**, 461.
Evans, I. N., and Dopita, M. A. 1985, *Ap. J. Suppl.*, **58**, 125.
Feast, M. W. 1968, *M.N.R.A.S.*, **140**, 345.
Feast, M. W., and Walker, A. R. 1987, *Ann. Rev. Astr. Ap.*, **25**, 345.
Gabler, R., Gabler, A., Kudritski, R. P., Puls, J., and Pauldrach, A. 1989, *Astr. Ap.*, **226**, 162.
Gathier, R., Pottasch, S. R., Goss, W. M., and van Gorkom, J. M. 1983, *Astr. Ap.*, **128**, 325.
Harrington, J. P. 1989, *IAU Symposium No. 131, Planetary Nebulae*, ed. S. Torres-Peimbert (Dordrecht: Kluwer), p. 157.
Henry, R. B. C. 1989, *M.N.R.A.S.*, **241**, 453.
Henry, R. B. C., Liebert, J., and Boroson, T. A. 1989, *Ap. J.*, **339**, 872.
Hummer, D. G., and Mihalas, D. 1970*a*, *M.N.R.A.S.*, **147**, 339.
———. 1970*b*, *J.I.L.A. Report*, No. 101, University of Colorado.
Kaler, J. B. 1978, *Ap. J.*, **225**, 527.
———. 1983, *IAU Symposium No. 103, Planetary Nebulae*, ed. D. R. Flower (Dordrecht: Reidel), p. 245.
———. 1985, *Ann. Rev. Astr. Ap.*, **23**, 89.
Lopez, J. A., and Meaburn, J. 1983, *M.N.R.A.S.*, **204**, 203.
McCarroll, R., Valiron, P., and Opradolce, L. 1983, *IAU Symposium No. 103, Planetary Nebulae*, ed. D. R. Flower (Dordrecht: Reidel), p. 187.
Meaburn, J., and Walsh, J. R. 1980, *M.N.R.A.S.*, **193**, 631.
Meatheringham, S. J., and Dopita, M. A. 1991, *Ap. J. Suppl.* in press.
Meatheringham, S. J., Dopita, M. A., Ford, H. C., and Webster, B. L. 1988, *Ap. J.*, **327**, 651.
Meatheringham, S. J., Dopita, M. A., and Morgan, D. H. 1988, *Ap. J.*, **329**, 166.
Monk, D. J., Barlow, M. J., and Clegg, R. E. S. 1988, *M.N.R.A.S.*, **234**, 583.
Morgan, D. H. 1984, *M.N.R.A.S.*, **208**, 633.
———. 1990, in preparation.
Morgan, D. H., and Good, A. R. 1985, *M.N.R.A.S.*, **213**, 491.
Noriega,Crespo, A., and McCall, M. 1989, in *IAU Symposium No. 131, Planetary Nebulae*, ed. S. Torres-Peimbert (Dordrecht: Kluwer), p. 228.
Péquignot, D., Aldrovandi, S. M. V., and Stasinska, G. 1978, *Astr. Ap.*, **63**, 313.
Pottasch, S. R., and Acker, A. 1989, *Astr. Ap.*, **221**, 123.
Preite-Martinez, A., and Pottasch, S. R. 1983, in *IAU Symposium No. 103, Planetary Nebulae*, ed. D. R. Flower (Dordrecht: Reidel), p. 547
Renzini, A., and Voli, M. 1981, *Astr. Ap.*, **94**, 175.
Russell, S. D., and Dopita, M. A. 1990, *Ap. J.*, in press.
Sanduleak, N., MacConnell, D. J., and Philip, A. G. D. 1978, *Pub. A.S.P.*, **90**, 621.
Shaw, R. A. 1989, in *IAU Symposium No. 131, Planetary Nebulae*, ed. S. Torres-Peimbert (Dordrecht: Kluwer), p. 473.
Schönberner, D. 1981, *Astr. Ap.*, **103**, 119.
Stoy, R. W. 1933, *M.N.R.A.S.*, **93**, 588.
Webster, B. L. 1975, *M.N.R.A.S.*, **173**, 437.
———. 1978, *M.N.R.A.S.*, **185**, 45P.
Wood, P. R., Bessell, M. S., and Dopita, M. A. 1986, *Ap. J.*, **311**, 632.
Wood, P. R., and Faulkner, D. J. 1986, *Ap. J.*, **307**, 659.
Wood, P. R., Meatheringham, S. J., Dopita, M. A., and Morgan, D. H. 1987, *Ap. J.*, **320**, 178.
Wood, P. R., and Zarro, D. M. 1981, *Ap. J.*, **247**, 247.

M. A. Dopita: Mt. Stromlo and Siding Spring Observatories, Private Bag, Weston Creek P.O., ACT 2611, Australia

S. J. Meatheringham: Laboratory for Astronomy and Solar Physics, NASA Goddard Space Flight Center, Code 680, Greenbelt, MD 20771